FRACTURE OF CONCRETE PLATES SUBJECTED TO ROTATING BIAXIAL STRESS

M.B. Nooru-Mohamed*, E. Schlangen*, J.G.M. van Mier*

Results are presented of displacement controlled tests on double-edge-notched concrete plates subjected to a rotating biaxial stress field. Two different load-paths were used and the path dependency is investigated. One of the load-paths is simulated numerically using a non-linear finite element package and compared with the experimental results. The results show that the presence of a lateral compressive shear load reduces the axial tensile capacity of the specimen. Furthermore a one to one relation exists between the lateral shear and the area of the compressive strut formed between the notches. It appears that the chosen load-path has a profound influence on the fracture mode. The formation of overlapping curved cracks shown in this paper is due to the rotation of the principal stress along the fracture front

INTRODUCTION

Brittle disordered materials like concrete show a degree of path dependency with respect to the load-path pursued. So far, a systematic study on path dependency in mixed-mode fracture of concrete is lacking except for a few attempts reported in (1,2). In the present study Double-Edge-Notched (DEN) concrete plates were subjected to two different load-paths. The reason for choosing various load-paths is to investigate in more detail the path dependency of mixed-mode fracture of concrete. The results can be used to tune the recently developed smeared rotating crack model (3). Using the DIANA (4) non-linear finite element code, one of the load-paths is simulated and a comparison is made with the experimental results.

EXPERIMENTAL TECHNIQUE

Specimens and Test Set-up

Square DEN concrete plates of dimension 200x200x50 mm with a notch depth of 25 mm were used throughout this study. The specimens were glued tothe biaxial test rig (5) as shown in Fig. 1a. The boundary conditions were such to allow for parallel end platen movement in the vertical and horizontal directions. The

* Delft University of Technology, Department of Civil Engineering, Stevin Laboratory, P.O. Box 5048, 2600 GA Delft, The Netherlands.

axial load P and lateral compressive shear P_s were applied as shown in Fig. 1a, resembling shear box experiments often adopted in rock mechanics. The global deformations measured with LVDTs ($\pm$ 1 mm) were used as feed back signal in the closed loop servo system (5), (6). In addition to that a total of 20 extensometers were mounted to the front and rear faces of the specimen for detailed crack measurements. All experiments were carried out using a 2 mm mortar mix. The mix-design is given in (6).

Load-paths

Two different load-paths were investigated in this study. In the first load-path three different shear values (-5 kN, -10 kN and maximum shear) were chosen.

Load-path 4a. A compressive shear P_s was applied to the specimen in displacement control until $P_s = 5$ kN. Subsequently, the lateral test control was changed to load control and an axial tensile load was applied in displacement control.

Load-path 4b/4c. In these cases the procedure was completely identical to that of load-path 4a, except that the shear load P_s was equal to 10 kN and the maximum shear force respectively.

Load-path 6a. An axial tensile and a lateral compressive shear load were applied to the specimen such that, a constant ratio of axial to lateral deformation prevailed throughout the test. The δ/δ_s ratio chosen was 1.0

RESULTS AND DISCUSSION

Load-path 4 results

Fig. 1b and c show the P_s-δ_s and P-δ diagrams for the three specimens corresponding to load-paths 4a, 4b and 4c. The shear loads chosen for these load-paths were -5, -10 and - 27.5 kN (maximum shear) respectively. From the local deformation measurements, it is evident that there was no crack initiation during shear for the load-path 4a and 4b experiments, and the P_s-δ_s diagrams are linear up till the prescribed P_s value. However, for the specimen 47-06 with the maximum shear, the P_s-δ_s diagram became non-linear at $P_s = -15$ kN and crack initiation occurred at the front left notch. When the shear load reached its maximum (-27.5 kN), the crack AB (Fig. 2c) propagated on the front face of the specimen 47-06. This caused an increase of δ (since LVDTs were mounted near the notch) during shear. Point A on the P-δ diagram for load-path 4c (Fig. 1c) corresponds to the axial deformation due to the lateral compressive shear. Also, at point A the axial tensile loading was activated, maintaining a constant lateral shear. As can be seen in Fig. 1c, soon after the activation of the axial tensile load, P became compressive. The highest axial tensile load (15 kN) was measured in the test with the low shear load of -5 kN. A 30% decrease in P occurred when P_s was increased from -5 kN to -10 kN. Obviously, the presence of a lateral compressive shear load significantly affects the axial tensile capacity of the specimen.

Fig. 2 shows the crack patterns for the load-path 4 experiments. There seems to exist a link between the lateral shear load and the area of the compressive struts (enclosed area between the two overlapping cracks). The specimen with the

maximum shear load (Fig. 2c) showed the largest strut, whereas the specimen with the lowest shear (Fig. 2a) gave the smallest strut size. In Fig. 2a the two overlapping cracks are more flattened as compared to Fig. 2c. In all these specimens the crack initiated at an angle nearly equivalent to 45 degrees. Rotation of the principal stresses has occurred in all three specimens of Fig. 2.

In Fig. 3, the crack opening paths δ-δ_s for the load-path 4 and 6a experiments are shown. The points of intersection between the various crack opening paths 4a, 4b, 4c and 6a are identified as A, B, and C. To check whether the behaviour of the specimens is path dependent, the corresponding loads P and P_s at the intersections A, B and C were retrieved from the experimental data. In Fig. 4, the difference between P ($= \Delta P$) and P_s ($= \Delta P_s$) for specimens pertaining to the two load-paths were plotted. Similarly (ΔP, ΔP_s) values for the points of intersection for load-paths 4 and 6 (circles in Fig. 3), 3 and 6 (triangles) and 5 and 6 (squares) were plotted in Fig. 3. Note that load-path 3 corresponds to compressive shear tests reported in (6). Load-path 5 is the same as load-path 4 until the maximum shear, but afterwards the axial tension was activated under constant lateral deformation instead of constant lateral load. It can be seen from Fig. 4 that the data points corresponding to the various load-paths discussed above were scattered throughout the diagram. The behaviour of the specimen would be path independent if $\Delta P = \Delta P_s = 0$, which is clearly not the case in the current tests.

Numerical Simulation

The behaviour of the DEN specimens under rotating stress was simulated using the finite element package DIANA(4). The element mesh adopted consisted of eight-noded elements which were integrated using the nine-point Gauss quadrature. Nonlinear analyses were carried out using the smeared crack concept (3). The material properties used in these simulations were: Young's modulus E $= 30000\ N/mm^2$, Poisson's ratio $\nu = 0.2$, tensile strength $f_{ct} = 3.3\ N/mm^2$, fracture energy $G_f = 100\ J/m^2$, crack band width $h = 12.5$ mm and the shear retention factor $\beta = 0$ ($= 0.001$ to avoid numerical problems). The stress crack opening diagram ($\sigma - \delta$) proposed in (7) was adopted. An incremental iterative procedure under load control is required to solve the nonlinear equations. The arc length method introduced in (8) was used to pass limit points of vertical tangent in the load displacement space.

Load-paths 4a and 4b experiments were simulated numerically and Figs. 5 and 6 show the calculated P_s-δ_s and P-δ diagrams. The calculated maximum load P for load-paths 4a and 4b exceeded the experimental peak load by 80% (Fig. 5). Also the post peak P-δ curves deviated from the actual experimental results (Figs. 1c and 6). The numerical analyses were stopped at $\delta = 45\ \mu m$ because convergence could not be obtained anymore. In Fig. 7 the calculated crack patterns are plotted for load-paths 4a and 4b. The calculated crack patterns deviated only slightly from each other and were both rather flat. The curved overlapping cracks found in the experiments were not found in the analyses.

The discrepancy between the numerical and the experimental results can possibly be explained from a poor reproduction of the stress gradient near the notch since rather large elements were used. The simulation includes mode I fracture only with no contribution due to shear. This might be another cause for the discrepancy between the experimental and numerical results. Further analyses are currently carried out.

CONCLUSIONS

(1) The axial tensile capacity of a DEN specimen is greatly reduced by the presence of a lateral compressive shear load.

(2) There is a one to one relation between the lateral compressive shear and the area of the compressive struts which formed between the two overlapping cracks between the two notches.

(3) The degree of curvature of the crack-trajectory depends on the magnitude of the lateral shear load.

(4) The fracturing of DEN specimens subjected to biaxial tension and shear is path dependent.

(5) There is a significant difference between the experiments and the numerical simulation using DIANA and which may warrant some modification in DIANA.

ACKNOWLEDGEMENTS

Thanks are due to Mr. G. Timmers for performing the experiments

REFERENCES

(1) Hassanzadeh, M., Eng. Frac. Mech., Vol. 35, No. 4/5, 1990,pp.845-853.

(2) Nissen, I., Rissverzahnung des Betons-Gegenseitige Risufervershiebungen und ubertragene Kräfte, Ph.D. thesis, Technical University of Munich, 1987.

(3) Rots, J.,Computational modeling of Concrete Fracture, Ph.D. Thesis, Delft University of Technology, The Netherlands, 1988.

(4) De Borst,R. et al., in Proc. Conf. on Eng. Software for Micro Computers, Venice, 1984, pp.435-446.

(5) van Mier, J.G.M., Nooru-Mohamed, M.B. and Schlangen, E., in "Application of Fracture Mechanics to Concrete Structures", Edited by L. Elfgren and S.P. Shah, Chapman & Hall, London\New York 1990 (In print)

(6) Nooru-Mohamed, M.B. and van Mier,J.G.M., in "Fracture of Concrete and Rock - Recent Developments", Edited by S.P. Shah et al., Elsevier, London/New York, 1989, pp. 458-464.

(7) Reinhardt, H.W., Cornelissen, H. A. W., Hordijk, D. A., J. Struct. Div., ASCE, Vol. 112, No, 11, 1986, pp.2462-2477.

(8) Riks, E., J. Appl. Mech. 39, 1972, pp. 1060-1066

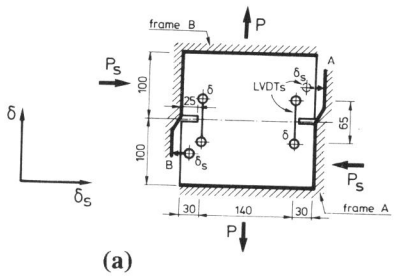

(a)

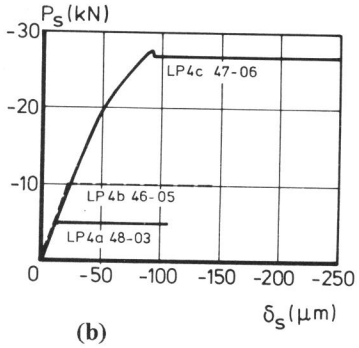

(b)

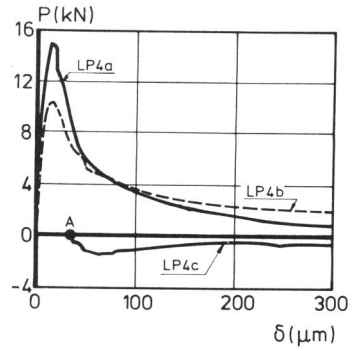

(c)

Figure 1. Specimen (a) P_s-δ_s (b) P-δ (c) diagrams for load-path 4

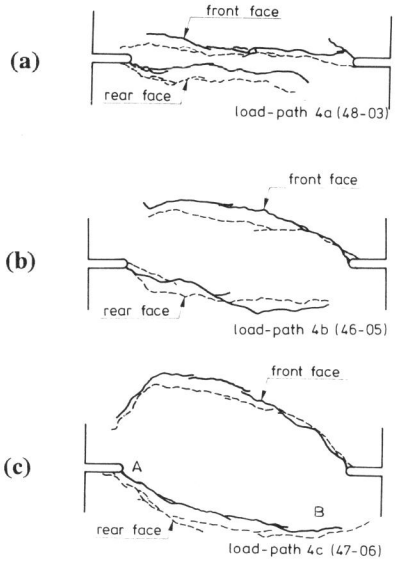

Figure 2. Crack patterns for load-path 4 experiments

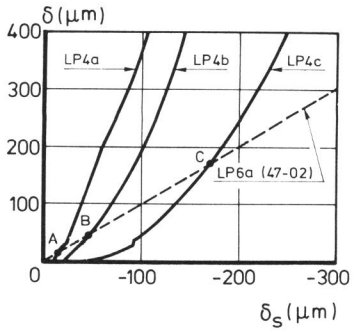

Figure 3. Crack opening path for load-path 4 and 6a experiments

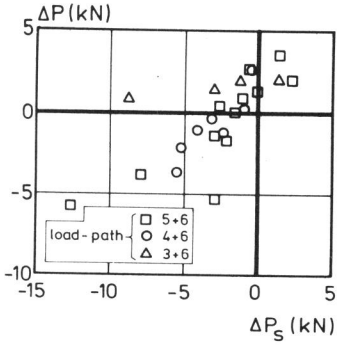

Figure 4. ΔP-ΔP_s plot

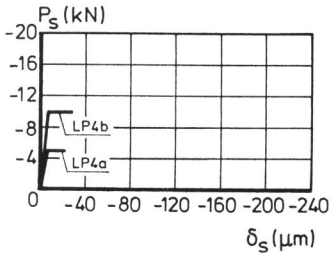

Figure 5. Simulated P_s-δ_s diagrams for load-path 4

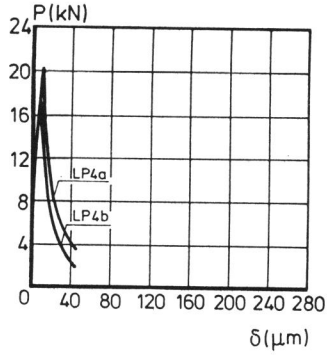

Figure 6. Simulated P-δ diagram for load-path 4

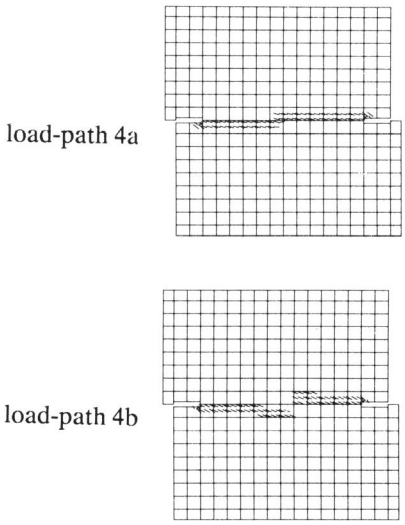

Figure 7. Simulated crack pattern for load-path 4a/4b